Coherent Transfer between Low-Angular-Momentum and Circular Rydberg States

A. Signoles,* E. K. Dietsche, A. Facon, D. Grosso, S. Haroche, J. M. Raimond, M. Brune, and S. Gleyzes†
Laboratoire Kastler Brossel, Collège de France, CNRS, ENS-PSL Research University, UPMC-Sorbonne Universités, 11, place Marcelin Berthelot, 75231 Paris Cedex 05, France
(Received 14 February 2017; published 23 June 2017)

We realize a coherent transfer between a laser-accessible low-angular-momentum Rydberg state and the circular Rydberg level with maximal angular momentum. It is induced by a radio frequency field with a high-purity σ^+ polarization resonant on Stark transitions inside the hydrogenic Rydberg manifold. We observe over a few microseconds more than 20 coherent Rabi oscillations between the initial Rydberg state and the circular level. We characterize these many-Rydberg-level oscillations and find them in perfect agreement with a simple model. This coherent transfer opens the way to hybrid quantum gates bridging the gap between optical communication and quantum information manipulations with microwave cavity and circuit quantum electrodynamics.

DOI: 10.1103/PhysRevLett.118.253603

The long-lived circular Rydberg levels (CRLs) are ideal tools for the quantum manipulation of microwave (mw) fields stored in high-Q 3D superconducting resonators. They led to early demonstrations of basic quantum information processing operations [1] and to the generation of nonclassical field state superpositions [2]. More recently, they have been instrumental in the exploration of fundamental cavity quantum electrodynamics (CQED) effects, such as quantum nondemolition (QND) measurements of the photon number [3] and quantum feedback [4]. Recent advances on the manipulation of Rydberg atoms near atom chips [5] indicate that they could be interfaced with the structures used in the flourishing field of circuit QED [6,7].

However, the photons used in mw cavity and circuit QED are unable to propagate over long-range transmission lines [8]. Optical to mw interfaces are thus the focus of an intense activity [9,10]. A new realm for mw quantum information manipulation would open if the CRLs could be coherently interfaced with optical photons, which are ideal long-haul quantum information carriers [11]. Unfortunately, the CRLs, with their large orbital quantum number $\ell = n - 1$ (n, principal quantum number), do not couple to optical photons.

In contrast, low-angular-momentum Rydberg states are accessible from the ground state by coherent laser excitation [12–14]. They were used for optical quantum information manipulations such as photon-photon gates based on single-photon optical nonlinearities due to the dipole blockade mechanism [15–18]. They could also lead to quantum gates entangling a mw photon with a collective hyperfine excitation in a ground state ensemble [19] and, hence, through the Duan-Lukin-Cirac-Zoller protocol [20], to gates entangling optical and mw photons. However, the short lifetime of these levels ($\simeq 100$ μs) sets limits on the fidelity and on their use in CQED experiments.

The missing link between mw and optical photons is a fast coherent transfer from a laser-accessible low-ℓ state to the CRLs. The most efficient CRL preparation technique so far involves a series of radio frequency (rf) transitions between Stark levels performed in an rapid adiabatic passage [21,22]. It thus requires a time much longer than the typical Rabi frequency on the rf transitions, which results in the accumulation of large dynamic phases. Their unavoidable fluctuations affect the coherence of the process. The crossed-fields technique [23,24], also based on an adiabatic passage, suffers from similar limitations.

In this Letter, we demonstrate a fast, coherent transfer between a low-ℓ state and the CRL. By coupling a Rydberg atom to a rf field with a well-defined polarization, we isolate in the Stark manifold with principal quantum number n a subset of states behaving as a large angular momentum $J \sim n/2$. We resonantly drive it and observe more than 20 coherent Rabi oscillations between the lowest (low-m) and uppermost (circular) energy states.

The experiment is performed on ^{85}Rb atoms in a static electric field $\boldsymbol{F} = F_0 z$, which partly lifts the Rydberg manifold degeneracy. Its levels can be sorted by their magnetic quantum number m (restricted to positive values here) [25]. For a hydrogen atom [see Fig. 1(a)], the Stark eigenstates are the parabolic states $|n, n_1, m\rangle$, where $0 \leq n_1 \leq n - m - 1$ labels states with the same m from bottom to top in a regularly spaced ladder. The lowest level of each m ladder ($n_1 = 0$) is midway between the lowest ones in the $m - 1$ ladder. The σ^+ rf transitions between these $n_1 = 0$ levels are thus all at the same angular frequency $\omega_n = (3/2)nF_0 e a_0/\hbar$ [26] (e, elementary charge; a_0, Bohr radius; $\omega_n/2\pi \approx 100$ MHz for $F_0 = 1$ V/cm and $n \approx 50$). A σ^+ rf field couples all the $n_1 = 0$ states from $m = 0$ up to the CRL. The subspace spanned by these levels is that of an angular momentum $\hat{\mathbf{J}}$, with $J = (n - 1)/2$ [27]. The CRL is the state $|J, m_J = J\rangle$ ("angular momentum up," north pole on a generalized Bloch sphere), and the lowest-m state $|n, 0, 0\rangle$ is $|J, m_J = -J\rangle$ ("angular momentum down," south pole) [28,29]. A resonant σ^+ rf

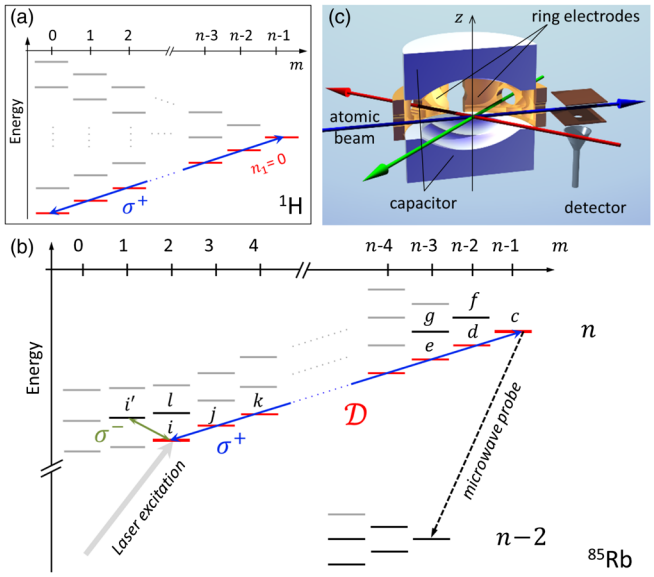

FIG. 1. (a) Scheme of the hydrogen Rydberg levels in the nth manifold in a static electric field (only states with $m \geq 0$ are shown). A σ^+ drive couples the $n_1 = 0$ levels (in red) from $m = 0$ to the CRL. (b) Scheme of Rb Rydberg levels. A ~ 2 V/cm electric field lifts the degeneracy of the nth Stark manifold. States with $m \geq 3$ are hydrogenoid, while lower m levels are affected by quantum defects. The ground state atoms are excited to the lower $m = 2$ state. A σ^+ polarized rf field couples $|n, i\rangle$ to an angular-momentum-like subspace $\mathcal{D}$ (red levels) via $\Delta m = +1$ transitions, leading to a transfer toward the CRL $|n, c\rangle$ (blue arrow). The population of each Stark level can be probed by selective mw transitions towards the corresponding level in the $n - 2$ manifold (dotted arrow). (c) Simplified experimental setup. Atoms from a thermal beam are optically excited at the center of the structure by lasers (red, 780 and 776 nm lasers; green, 1258 nm laser). A set of electrodes is used to apply static and rf electric fields. After a $\sim$230 μs time of flight, the atoms are detected out of the structure by field ionization.

drive at frequency $\omega_{\rm rf} = \omega_n$ induces a rotation of $\hat{\mathbf{J}}$ between the north and south poles at a frequency $\Omega_{\rm rf}/2\pi = (3/2)nea_0E^+_{\rm rf}/h$, where $E^+_{\rm rf}$ is the electric field amplitude. This rotation maps the angular-momentum down state into the CRL in a time $\pi/\Omega_{\rm rf}$.

For rubidium [Fig. 1(b)], the levels with $m < 3$ are shifted by the quantum defects due to the finite size of the atomic core [25]. The levels with $m \geq 3$ arrange in the hydrogenic pattern and are connected by degenerate σ^+ transitions [blue arrow in Fig. 1(b)]. For $m = 2$, the $|n, n_1 = 0, m = 2\rangle$ state is shifted far away from the manifold. However, a fortunate coincidence makes the rf transition between the $|n, n_1 = 1, m = 2\rangle = |n, i\rangle$ state and the first hydrogenic $|n, n_1 = 0, m = 3\rangle = |n, j\rangle$ level nearly degenerate with the transitions toward $|n, c\rangle$. Hence, only the two lowest states $m = 0$, 1 are nonresonant. The transfer from $|n, i\rangle$ to the CRL is a nearly π rotation of the hydrogenic angular momentum $\hat{\mathbf{J}}$, through a subset $\mathcal{D}$ of its levels [in red in Fig. 1(b)].

The experiment takes place in a capacitor producing $\boldsymbol{F}$, surrounded by four ring electrodes, on which we apply the rf signal at $\omega_{\rm rf}/2\pi = 230$ MHz and dc potentials [Fig. 1(c)]. It is crossed by a rubidium beam (atomic velocity 250 m/s). Atoms are excited from the $5S$ ground state by laser beams resonant on the transitions $5S_{1/2} \rightarrow 5P_{3/2}$ (780 nm), $5P_{3/2} \rightarrow 5D_{5/2}$ (776 nm), and $5D_{5/2} \rightarrow nF$, $m = 2$ (1258 nm). The 780 and 776 nm beams are σ^+ polarized and collinear with the quantization axis, defined by a dc field (0.23 V/cm) applied across the ring electrodes during the 1 μs pulsed laser excitation. The 1258 nm beam is perpendicular to the others, with π polarization. After the excitation, a potential is switched on on the capacitor in 1 μs, resulting in a field $\boldsymbol{F} = F_0\boldsymbol{z}$ with $F_0 \sim 2$ V/cm and preparing the initial state $|n, i\rangle$ [22]. The atoms finally drift out of the capacitor towards a field-ionization detector. It resolves the CRL from the initial state but does not resolve them from levels with similar energies. In order to selectively detect neighboring levels $|n, p\rangle$ with $p = i, i', j, k, l, c, d, e, f, g$ [Fig. 1(b)], we use selective mw probe pulses, transferring $|n, p\rangle$ into another manifold resolved by the detector.

The rf transfer from $|n, i\rangle$ to $|n, c\rangle$ requires a pure rf σ^+ polarization, avoiding transitions with $\Delta m = -1$ and confining the evolution in $\mathcal{D}$. By applying on the ring electrodes 230 MHz signals with proper phases and amplitudes, we can generate a pure σ^+ field in the center of the capacitor. Because of mismatches in the driving line transmissions and of the capacitive coupling between electrodes, these phases and amplitudes cannot be predetermined. We use an optimization procedure, based on the measurement of the $\sigma^\pm$ fields. We set the static field to $F_0 = 1.76$ V/cm, so that the σ^- rf is resonantly coupled to the $|n = 52, n_1 = 1, m = 2\rangle - |n = 52, n_1 = 3, m = 1\rangle$ transition [$|52, i\rangle - |52, i'\rangle$ in Fig. 1(b)]. All other transitions from $|52, i\rangle$ or $|52, i'\rangle$ are out of resonance due to the quantum defects. The induced Rabi oscillations are at a frequency $\Omega^-_{ii'}/2\pi = \sqrt{2}d_{ii'}E^-_{\rm rf}/h$, where $E^-_{\rm rf}$ is the σ^- amplitude and $d_{ii'}$ the dipole matrix element. To measure the σ^+ amplitude, we align the electric field along the $-z$ direction instead of $+z$. The atom is then prepared in the $m = +2$ state with respect to the reversed Oz axis (noted $-Oz$). The transition between $|52, i\rangle$ and $|52, i'\rangle$ is driven by the σ^- polarization with respect to $-Oz$, i.e., σ^+ with respect to Oz.

The optimization is detailed in Ref. [30]. Figure 2(a) presents the Rabi oscillation between $|52, i\rangle$ and $|52, i'\rangle$ due to the weak σ^- component. A fit (solid red line) yields $\Omega^-_{ii'}/2\pi = 107 \pm 25$ kHz. Figure 2(b) presents the Autler-Townes doublet induced by the strong σ^+ rf probed on the $|52, i\rangle - |51, n_1 = 0, m = 3\rangle$ mw transition, leading to $\Omega^+_{ii'}/2\pi = \sqrt{2}d_{ii'}E^+_{\rm rf}/h = 30.0$ MHz. The polarization purity is remarkable, $E^-_{\rm rf}/[(E^+_{\rm rf})^2 + (E^-_{\rm rf})^2]^{1/2} = 0.36 \pm 0.08\%$, consistent with the inhomogeneity of the rf over

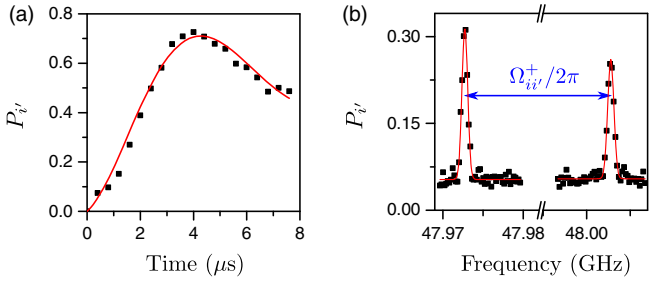

FIG. 2. (a) Rabi oscillation induced by the σ^- polarization component of the rf field on the $|52, i\rangle \rightarrow |52, i'\rangle$ transition (electric field along the $+z$ direction). Population $P_{i'}$ of $|52, i'\rangle$ versus the rf pulse duration t (dots). The fit (red line) provides $\Omega^{-}_{ii'}/2\pi = 107 \pm 25$ kHz. (b) Autler-Townes doublet of the $|52, i\rangle \rightarrow |52, i'\rangle$ transition (electric field along $-z$) dressed by the σ^+ rf field. Points are experimental; red lines are Gaussian fits leading to $\Omega^{+}_{ii'}/2\pi = 30.0$ MHz.

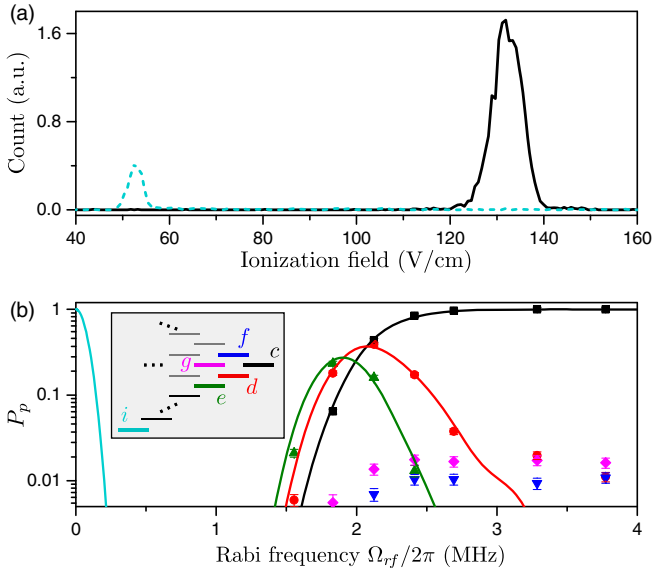

FIG. 3. Adiabatic passage in the $n = 51$ manifold. (a) Field ionization spectra (signal versus the ionization detector field) of the initial state $|51, i\rangle$ (dashed cyan line) and after the adiabatic passage (solid black line). (b) Populations P_p for $p = i, c, d, e, f, g$ of the states $|51, p\rangle$ (color code for level identification in the inset) as a function of the Rabi frequency $\Omega_{\rm rf}/2\pi$. Dots are experimental with statistical error bars. Solid lines are the result of a numerical simulation of the full Hamiltonian evolution.

the atomic sample size ($\simeq$1 mm) calculated using the SIMION software package.

As a first test, we use the optimized rf field to prepare the CRL by the adiabatic transfer method [22]. To allow us to use calibrated mw probes [30], we perform this experiment in the 51 manifold. We initially prepare the atoms in $|51, i\rangle$ and set the electric field to $F_0 = 2.45$ V/cm so that $\delta = \omega_{51} - \omega_{\rm rf} = 2\pi \times 10$ MHz. The rf field power is ramped up in 1 μs. The electric field F_0 is then linearly decreased to 2.24 V/cm ($\delta = -2\pi \times 10$ MHz) in 1.5 μs, so that ω_{51} crosses the resonance. The rf is finally switched off in 1 μs. We record the number of detected atoms as a function of the ionization field [Fig. 3(a)]. The cyan dashed line presents the ionization signal of the initial $|51, i\rangle$ level. The black line shows that the signal after the adiabatic passage is centered on the $|51, c\rangle$ ionization field. From the residual number of atoms detected at the ionization field of $|51, i\rangle$, we estimate the transfer efficiency to be $> 98\%$. The difference of height between the cyan and black signals provides the relative detection efficiency, $\eta_0 = 0.23$, between $|51, i\rangle$ and $|51, c\rangle$. Its low value is mainly due to the difference of level lifetime.

We investigate the adiabatic transfer as a function of $\Omega_{\rm rf}$. The populations of levels c, d, e, f, and g (points in Fig. 3 with statistical error bars) are measured with calibrated mw probes [30]. The conversion factor between $\Omega_{\rm rf}$ and $E^{+}_{\rm rf}$ is determined from the measurement of $\Omega^{+}_{ii'}$ (Fig. 2). The data are in excellent agreement with the result of a numerical simulation of the ideal evolution in a pure σ^+ field (solid lines). For $\Omega_{\rm rf} > 3$ MHz, the CRL population is remarkably close to one. The total population of levels d, e, f, and g is at most 5% (part of this population is overestimated due to mw probe imperfections). This demonstrates the excellent rf polarization control achieved here.

We now investigate the resonant rf regime, which provides the coherent transfer between a low-ℓ state and the CRL. The field F_0 is adjusted to 2.35 V/cm corresponding to $\omega_{51} \approx \omega_{\rm rf}$. For a fixed rf amplitude, we scan the rf pulse duration $\Delta t_{\rm rf}$ and measure the state populations as above. The circular state population P_c [dots in Fig. 4(a) with statistical error bars] exhibits periodic peaks. They reveal 23 Rabi oscillations over 6 μs, demonstrating the atomic evolution coherence. A fit of these data with a numerical simulation of the Hamiltonian evolution in a pure σ^+ field (solid line) calibrates the rf Rabi frequency $\Omega_{\rm rf} = 3.52$ MHz and the effective rf pulse duration, slightly different (≈ 68 ns) from $\Delta t_{\rm rf}$ due to the rise and fall times of the electronic drive.

In Fig. 4(b), we plot the populations P_p for $p = i, c, d, e, f, g$ around the second CRL population maximum. We observe for P_d and P_e the expected double peak structure, typical of a multilevel Rabi oscillation. Figure 4(c) presents the calculated (bars) and measured (open circles) population at $\Delta t_{\rm rf} = 0.45$ μs. The deviations with respect to the hydrogen atom model become more important with time, since the quantum defects affect the evolution each time the atom returns to low-m states. Figure 4(d) shows an enlargement of the evolution at long times (dots) together with the numerical prediction (solid line) and Fig. 4(e) the calculated (bars) and measured (open circles) populations at $\Delta t_{\rm rf} = 4.26$ μs. The agreement between theory and experiment remains excellent up to

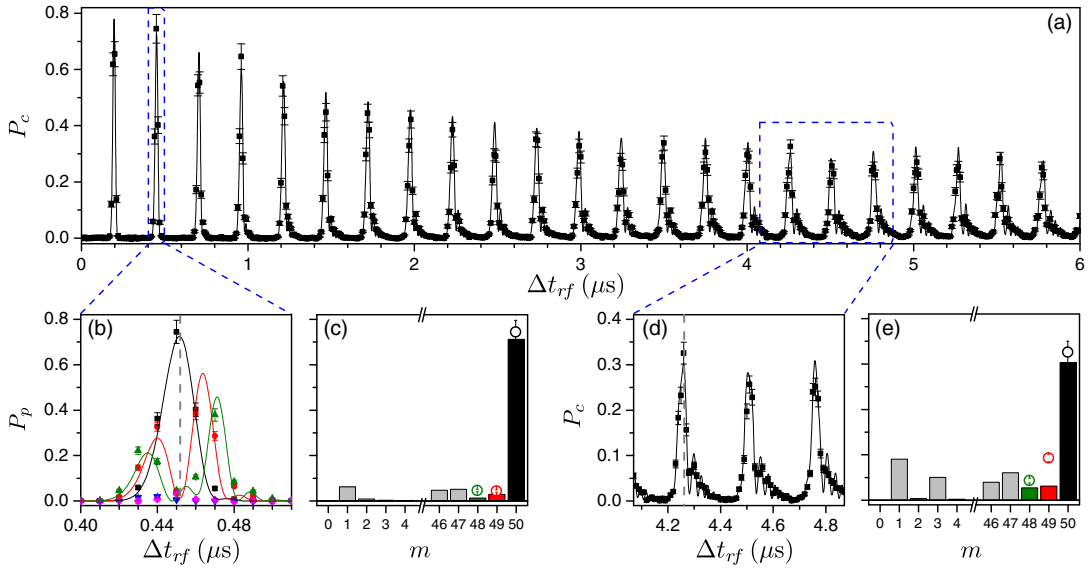

FIG. 4. Dynamics of the atomic state for a rf pulse duration Δt_{rf}. (a) Long time scale evolution of the CRL population P_c (dots). The solid line is the result of a numerical simulation, with $\Omega_{\mathrm{rf}}/2\pi = 3.52$ MHz and a rf pulse shortened by 68 ns to model the rise and fall times of the driving electronics. (b) Populations P_p for $p = c, d, e, f, g$ around the second maximum of P_c (same color conventions as in Fig. 2). Dots are experimental, and solid lines are the results of the simulation. (c) Calculated (bars) and measured (open circles) populations P_p at the top of the second CRL population maximum. (d) Enlargement of (a) around three late CRL population maxima. (e) Calculated (bars) and measured (open circles) populations P_p at the top of the first CRL population maximum in (d). For all panels, the experimental error bars correspond to the statistical fluctuations.

large Δt_{rf} values, demonstrating the coherence of the oscillation over long times.

This experiment demonstrates an efficient coherent Rabi oscillation from the low-m state $|n, i\rangle$ to the CRL $|n, c\rangle$ within 200 ns. The transfer rate ($\simeq$80%) is mainly explained by the absence of the $m = 0$, 1 states in the angular-momentum ladder and to the residual quantum defect of $m = 2$. These residual imperfections could be reduced by tailoring the amplitude and the frequency of the rf field via optimal control [31]. The much higher final fidelity will be limited by the residual electric field inhomogeneities.

This coherent transfer opens a realm of new possibilities for the thriving field of Rydberg atoms, in which experiments are oftentimes limited by the finite lifetime of the low-m states. It also opens the way to a phase gate between an optical and a mw photon, along the lines proposed in Ref. [19] for low-angular-momentum Rydberg states. It relies on a dense ensemble of ground state ^{87}Rb atoms, prepared in the $F = 1$ hyperfine ground state and held by a dipole trap inside a high-quality open Fabry-Perot mw resonator [1] tuned to the $|50, c\rangle - |51, c\rangle$ transition. An incoming optical photon is transformed into a collective excitation in the $F' = 2$ ground state [20]. A laser pulse coherently transfers this excitation into the $|50, i\rangle$ Rydberg level, immediately cast onto the $|50C\rangle$. The atom is then coupled to the cavity for the duration of a resonant 2π Rabi rotation, resulting in a conditional π phase shift for the atom iff the cavity contains one mw photon [32]. This π shift is brought back to the F' ground state by the time-reversed excitation process and converted back into an optical photon. All the components of this innovative hybrid photon-photon quantum gate have now been tested separately, including the transfer between the low ℓ and the CRL. Assembling these components would bridge the gap between optical quantum communication and quantum information manipulations based on mw cavity and circuit quantum electrodynamics.

We acknowledge funding by the European Union under the European Research Council project "DECLIC" (Project No. 246932) and the Research and Innovation action project "RYSQ" (Project No. 640378).

*Physikalisches Institüt, Universität Heidelberg, Im Neuenheimer Feld 226, 69120, Heidelberg, Germany.
†gleyzes@lkb.ens.fr

[1] J. M. Raimond, M. Brune, and S. Haroche, Rev. Mod. Phys. **73**, 565 (2001).
[2] M. Brune, E. Hagley, J. Dreyer, X. Maître, A. Maali, C. Wunderlich, J. M. Raimond, and S. Haroche, Phys. Rev. Lett. **77**, 4887 (1996).
[3] C. Guerlin, J. Bernu, S. Deléglise, C. Sayrin, S. Gleyzes, S. Kuhr, M. Brune, J.-M. Raimond, and S. Haroche, Nature (London) **448**, 889 (2007).
[4] C. Sayrin *et al.*, Nature (London) **477**, 73 (2011).
[5] R. Celistrino Teixeira, C. Hermann-Avigliano, T. L. Nguyen, T. Cantat-Moltrecht, J. M. Raimond, S. Haroche,

S. Gleyzes, and M. Brune, Phys. Rev. Lett. **115**, 013001 (2015).
[6] S. D. Hogan, J. A. Agner, F. Merkt, T. Thiele, S. Filipp, and A. Wallraff, Phys. Rev. Lett. **108**, 063004 (2012).
[7] M. H. Devoret and R. J. Schoelkopf, Science **339**, 1169 (2013).
[8] H. Wang *et al.*, Phys. Rev. Lett. **106**, 060401 (2011).
[9] D. Maxwell, D. J. Szwer, D. Paredes-Barato, H. Busche, J. D. Pritchard, A. Gauguet, M. P. A. Jones, and C. S. Adams, Phys. Rev. A **89**, 043827 (2014).
[10] R. W. Andrews, R. W. Peterson, T. P. Purdy, K. Cicak, R. W. Simmonds, C. A. Regal, and K. W. Lehnert, Nat. Phys. **10**, 321 (2014).
[11] J. I. Cirac and H. J. Kimble, Nat. Photonics **11**, 18 (2017).
[12] T. A. Johnson, E. Urban, T. Henage, L. Isenhower, D. D. Yavuz, T. G. Walker, and M. Saffman, Phys. Rev. Lett. **100**, 113003 (2008).
[13] M. Reetz-Lamour, T. Amthor, J. Deiglmayr, and M. Weidemüller, Phys. Rev. Lett. **100**, 253001 (2008).
[14] Y. Miroshnychenko, A. Gaëtan, C. Evellin, P. Grangier, D. Comparat, P. Pillet, T. Wilk, and A. Browaeys, Phys. Rev. A **82**, 013405 (2010).
[15] T. Peyronel, O. Firstenberg, Q.-Y. Liang, S. Hofferberth, A. V. Gorshkov, T. Pohl, M. D. Lukin, and V. Vuletić, Nature (London) **488**, 57 (2012).
[16] V. Parigi, E. Bimbard, J. Stanojevic, A. J. Hilliard, F. Nogrette, R. Tualle-Brouri, A. Ourjoumtsev, and P. Grangier, Phys. Rev. Lett. **109**, 233602 (2012).
[17] S. Baur, D. Tiarks, G. Rempe, and S. Dürr, Phys. Rev. Lett. **112**, 073901 (2014).
[18] D. Paredes-Barato and C. S. Adams, Phys. Rev. Lett. **112**, 040501 (2014).
[19] J. D. Pritchard, J. A. Isaacs, M. A. Beck, R. McDermott, and M. Saffman, Phys. Rev. A **89**, 010301(R) (2014).
[20] L. M. Duan, M. D. Lukin, J. I. Cirac, and P. Zoller, Nature (London) **414**, 413 (2001).
[21] R. G. Hulet and D. Kleppner, Phys. Rev. Lett. **51**, 1430 (1983).
[22] P. Nussenzveig, F. Bernardot, M. Brune, J. Hare, J. M. Raimond, S. Haroche, and W. Gawlik, Phys. Rev. A **48**, 3991 (1993).
[23] D. Delande and J. Gay, Europhys. Lett. **5**, 303 (1988).
[24] J. Hare, M. Gross, and P. Goy, Phys. Rev. Lett. **61**, 1938 (1988).
[25] T. F. Gallagher, *Rydberg Atoms*, Cambridge Monographs on Atomic, Molecular and Chemical Physics (Cambridge University Press, Cambridge, England, 1994).
[26] H. Bethe and E. Salpeter, *Quantum Mechanics of One-and Two-Electron Atoms, 1957* (Springer, Berlin, 1977).
[27] R. Lutwak, J. Holley, P. P. Chang, S. Paine, D. Kleppner, and T. Ducas, Phys. Rev. A **56**, 1443 (1997).
[28] M. Englefield, *Group Theory and the Coulomb Problem* (Wiley-Interscience, New York, 1972).
[29] J.-C. Gay, D. Delande, and A. Bommier, Phys. Rev. A **39**, 6587 (1989).
[30] See Supplemental Material at http://link.aps.org/supplemental/10.1103/PhysRevLett.118.253603 for a description of the polarization optimization procedure and the calibration of the microwave probe efficiency.
[31] J. P. Palao, D. M. Reich, and C. P. Koch, Phys. Rev. A **88**, 053409 (2013).
[32] G. Nogues, A. Rauschenbeutel, S. Osnaghi, M. Brune, J. M. Raimond, and S. Haroche, Nature (London) **400**, 239 (1999).